Satellite-assisted quantum communication with single photon sources and atomic memories

V. Domínguez Tubío [1,2] M. Badás Aldecocea [3] J. van Dam [1,2,4] A. S. Sørensen [5] and J. Borregaard [1,6]

[1]*QuTech, Delft University of Technology, 2628 CJ Delft, The Netherlands*

[2]*Kavli Institute of Nanoscience, Delft University of Technology, 2628 CJ Delft, The Netherlands*

[3]*Space Engineering Department, Delft University of Technology, 2629 HS Delft, The Netherlands*

[4]*Quantum Computer Science, EEMCS, Delft University of Technology, 2628 CJ Delft, The Netherlands*

[5]*Center for Hybrid Quantum Networks (Hy-Q), Niels Bohr Institute, University of Copenhagen, Blegdamsvej 17, DK-2100 Copenhagen, Denmark*

[6]*Department of Physics, Harvard University, Cambridge, Massachusetts 02138, USA*

(Received 19 November 2024; accepted 11 July 2025; published 29 January 2026)

Satellite-based quantum repeaters are a promising means of reaching global distances in quantum networking due to the polynomial decrease of optical transmission with distance in free space, in contrast to the exponential decrease in optical fibers. We propose a satellite-based quantum repeater architecture with trapped individual atomic qubits, which can serve both as quantum memories and true single-photon sources. This hardware allows for nearly deterministic Bell measurements and exhibits long coherence times, without the need for costly cryogenic technology in space. We develop a detailed analytical model of the repeater, which includes the main imperfections of the quantum hardware and the optical link, assuming high-altitude ground stations, and consequently working in a regime of weak atmospheric turbulence. Our model allows us to estimate that high-rate and high-fidelity entanglement distribution can be achieved over intercontinental distances. In particular, we find that high-fidelity entanglement distribution over thousands of kilometres at a rate of 100 Hz can be achieved with orders of magnitude fewer memory modes than conventional architectures based on optical Bell state measurements.

DOI: 10.1103/z1vn-11m5

I. INTRODUCTION

The implementation of a quantum internet opens a range of new opportunities for secure communication [1–3], enhanced sensing networks [4–6], and distributed quantum computing [7]. To exploit these opportunities in applications such as protecting and optimizing large-scale power distribution networks [8] or probing fundamental constants and geodesy [9], it is necessary to extend the range of quantum networks to distances of thousands of kilometers.

To carry out quantum communication, we need to use photons to transmit quantum information. However, transmission loss of an optical quantum signal cannot be compensated with standard classical amplification techniques due to the quantum no-cloning theorem [10]. Instead, quantum repeaters have been proposed, where the total distance is divided into smaller segments over which direct transmission is feasible. The segments are then combined either through quantum teleportation [11,12] or quantum error correction [13,14] at the repeater nodes to enable faithful transmission over the total distance.

For optical fiber-based quantum repeaters, the transmission between the repeater nodes decreases exponentially with distance, and hundreds of repeater nodes are required to cover distances at the continental scale. Alternatively, fiber-based connections can be replaced with satellite-assisted free-space optical links where transmission decreases only polynomially with the distance [15–21]. For continental scales, this can reduce the required number of repeater nodes by orders of magnitude, making up for the arguably higher cost of space-based quantum repeater nodes.

Quantum key distribution (QKD) has already been demonstrated with the Micius satellite performing as a trusted node for distances ranging from 500 to 7000 km [22,23]. However, assuming that the satellite is a trusted node poses a security concern.

In a more advanced approach, entanglement-based QKD was achieved without relying on a trusted node, spanning distances of up to 1200 km [24]. In this case, the satellite served as a source of entangled photon pairs, paving the way for future entanglement-based quantum networks. Reaching larger distances by direct transmission, however, requires a high-orbit satellite due to the limitation of the line of sight of the ground receivers. This substantially increases the transmission loss, making high-rate quantum communication extremely challenging. Alternatively, multiple low-orbit satellites can operate in a quantum repeater architecture to efficiently compensate for the transmission loss and ensure line of sight between distant locations [16–18].

Previous theoretical work on satellite-based quantum repeaters assumes the use of probabilistic optical Bell state measurements (BSMs) [16], which require multiplexing of thousands of memory modes to reach high-rate

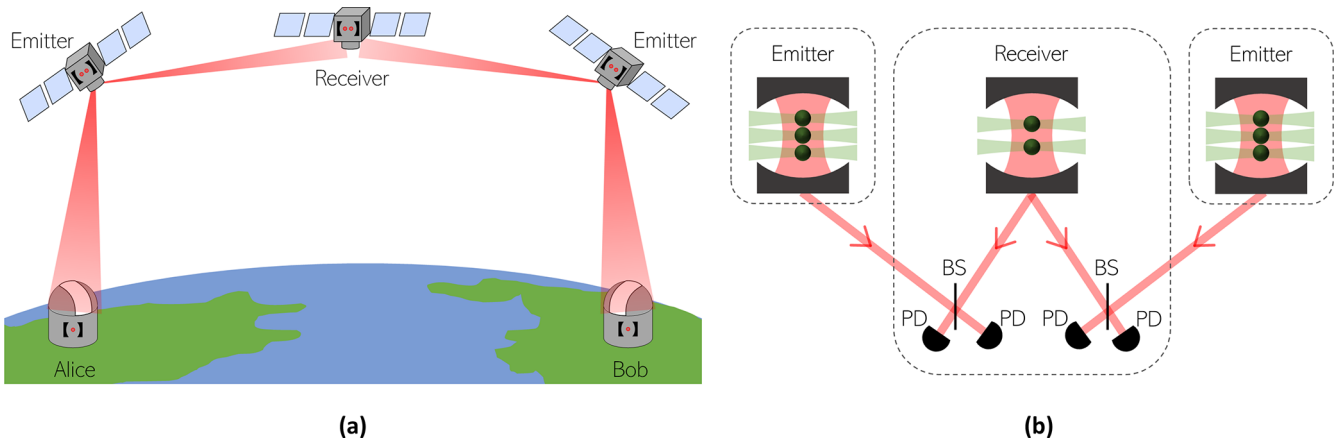

FIG. 1. Schematic diagram of the proposed scheme. (a) We consider a downlink scenario where the photons are transmitted from the end satellites to the ground stations. Each of the satellites contains quantum memories, and entanglement swaps are performed on the satellites to link the segments of the repeater (satellite-satellite or satellite-ground stations) once entanglement has been established. (b) Probabilistic Bell state measurement after entanglement generation. The atom-photon entanglement generated through the emission of a photon from an atom is swapped to atom-atom entanglement within a receiver satellite by means of a linear optics Bell state measurement. This is done using a 50/50 beam splitter (BS) and single-photon detectors. As shown in the figure, emitter telescopes typically need more memory modes than the receiver telescope because we are operating in a low transmission probability regime.

communication over global distances. Additionally, the availability of on-demand entangled photon pair sources is often assumed [16,18–20], which remains an outstanding technological challenge [25]. Promising candidate systems are solid-state semiconductor quantum dots [26], which require cryogenic temperatures to function, or multiplexing of spontaneous parametric down-conversion (SPDC) sources [27] and single-photon sources [28].

We propose a satellite-assisted quantum repeater protocol based on trapped individual atomic qubits. Individually trapped Alkali atoms can both function as efficient single-photon sources [29] and atomic memories due to their long coherence times [30,31]. Furthermore, they enable nearly deterministic BSMs through Rydberg-mediated two-atom gates [32–34] and the possibility of scaling to hundreds of qubits per repeater node [35,36]. Additionally, laser-cooling of the atoms is sufficient to ensure long coherence times, which avoids the need for costly cryogenic technology in space.

We develop a detailed analytical model of the repeater protocol that considers the main imperfections of both the quantum hardware and the optical link budget. For the latter, we assume high-altitude ground stations, allowing us to operate in a weak atmospheric turbulence regime. In contrast to Monte Carlo-based simulations [18], the analytical model allows us to efficiently simulate long chains of quantum repeater nodes. We show that, for realistic satellite parameters and quantum hardware errors, we can get high-fidelity ($\geqslant 0.9$) entanglement distribution rates of 100 Hz over continental distances of up to 1500 km using five satellites with less than 200 quantum memory modes per satellite.

II. RESULTS

A. Architecture

We consider a downlink scenario where photons are sent from the end satellites to the ground stations, which is more robust to atmospheric turbulence than the reverse uplink scenario [17,37]. A high-level sketch of a three-node repeater is shown in Fig. 1(a). The quantum repeater consists of different types of satellites. Some satellites act as emitters, sending photons to their neighboring satellites or to the ground station. Others are receivers that collect the photons sent by the emitter satellites. Both types of satellites are equipped with atomic quantum memories and act as quantum repeater nodes, as shown in Fig. 1(b). When adding more satellites, we always ensure an odd number to maintain the structure of the receiver and emitter satellites.

To distribute entanglement between the ground stations, atom-photon entanglement is generated at the repeater stations through pulsed excitation of the atoms. The generated photons are sent from the emitter nodes to the receiver ones, where the atom-photon entanglement is swapped to atom-atom entanglement by means of a linear optics BSM. Once entanglement between two neighboring elementary links has been successfully heralded, a nearly deterministic entanglement swap operation is performed through Rydberg-mediated atom-atom interactions. If the entanglement generation is successful in all elementary links, the two ground states will share an entangled pair.

B. Entanglement generation

For the generation of atom-atom entanglement, we consider a "two-click" protocol [38], where each atom is entangled with a time-bin encoded single photon through pulsed excitation. This is then swapped to atom-atom entanglement by a linear optics Bell measurement. We focus on this scheme since it only requires phase stability on the timescale of the time-bin separation and does not have the fundamental trade-off between rate and fidelity of "single-click" protocols [39]. Furthermore, we consider a scenario where the entanglement swapping happens at a heralding station placed on the receiving satellite. The loss will thus only affect one of the photons, and the usual advantage of the single-click protocol

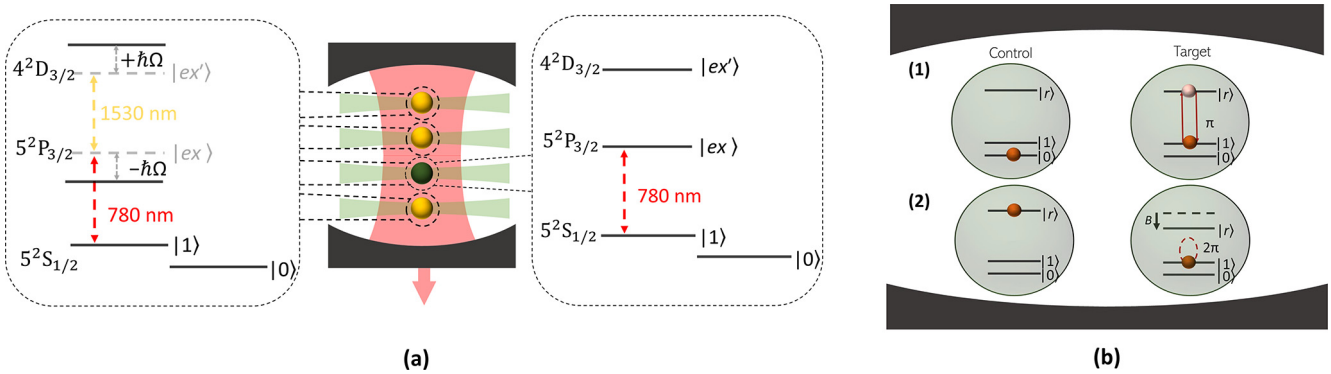

FIG. 2. Individually trapped atoms in a cavity as the main hardware. (a) The quantum memories chosen are Rubidium (Rb) atoms in a cavity, which also work as emitters. With a laser resonant with the $|1\rangle \rightarrow |ex\rangle$ transition, the atom is excited to the $|ex\rangle$ state from which it will decay back to the $|1\rangle$ state with the emission of a photon. To selectively address only one atom in an entangling attempt, the other atoms are shifted out of resonance through strong driving of the $|ex\rangle \rightarrow |ex'\rangle$ transition. (b) Nearly deterministic Bell state measurement. After the elementary links are entangled, a nearly deterministic Bell state measurement is carried out to distribute entanglement between Alice and Bob. The latter is performed by applying a CNOT gate between the atoms and a Hadamard gate in the control atom. To perform the 2-qubit gate, we exploit the well-known Rydberg blockade: The $|1\rangle \rightarrow |r\rangle$ transition of the target atom is resonant with our driving field if (1) the control atom is in state $|0\rangle$ but (2) shifted out of resonance by the Rydberg interaction if the control atom is in state $|r\rangle$.

of having a higher rate for long distances is thus not applicable in this scenario.

We now describe the steps of the entanglement generation in more detail. Figure 2(a) shows how individual atoms are trapped with optical tweezers inside macroscopic, near-concentric optical cavities [35,36,40]. Throughout this paper, we focus on an implementation with Rubidium (Rb) atoms, though other alkali atoms such as cesium could also be used. The closed optical transition between the $5S_{1/2}$, $|F = 2, m_F = 2\rangle$ ground state and the $5P_{3/2}$, $|F' = 3, m_{F'} = 3\rangle$ excited state in ^{87}Rb allows for spin-photon entanglement through pulsed excitation. For simplicity, we first describe this process for a single atom and then discuss how to perform the operation for a collection of atoms.

First, the atom is prepared in a superposition of the spin states,

$$|\phi\rangle = \frac{1}{\sqrt{2}}(|0\rangle + |1\rangle), \tag{1}$$

by means of standard optical pumping and two-photon Raman driving [30,41]. We imagine that $|0\rangle = |F = 1, m_F = 1\rangle$ and $|1\rangle = |F = 2, m_F = 2\rangle$ in the $5^2S_{1/2}$ ground state manifold. Next, a short optical π-pulse is applied to induce the transition, $|1\rangle \rightarrow |ex\rangle$, where $|ex\rangle = |F' = 3, m'_F = 3\rangle$ in the excited $5^2P_{3/2}$ manifold. The excited state will subsequently decay back to $|1\rangle$ by emission of an early cavity photon, $|e\rangle$. Next, two-photon Raman driving is used to flip the population of the ground states, that is, $|0\rangle \leftrightarrow |1\rangle$, after which a second optical π-pulse is applied, resulting in the emission of a late photon, $|l\rangle$ if the atom is in the $|1\rangle$ state. Ideally, this procedure results in the spin-photon entangled state

$$|\psi\rangle_{sp} = \frac{1}{\sqrt{2}}(|0\rangle|e\rangle + |1\rangle|l\rangle). \tag{2}$$

When performing this operation on a collection of atoms, it is important to prevent the emission from one atom from interfering with another. To this end, we propose to operate in a sequential manner where all atoms are initially prepared in the state $(|0\rangle + |1\rangle)/\sqrt{2}$ and then addressed sequentially with the optical π-pulse for the generation of atom-photon entanglement. An additional laser at 1530 nm addressing the transition between the $5^2P_{3/2}$ and $4^2D_{3/2}$ excited manifolds is applied to all atoms except the one subject to the optical π pulse. Specifically, a π-polarized laser will couple the excited $|ex\rangle$ to the $|ex'\rangle = |F'' = 3, m_{F''} = 3\rangle$ hyperfine level of the $4^2D_{3/2}$ manifold. This is done to effectively shift the $|1\rangle \leftrightarrow |ex\rangle$ transition out of resonance for the other atoms, since the excited dressed states will be detuned from the cavity resonance by $\pm\hbar\Omega$, where Ω is the Rabi frequency of the laser-driven $|ex\rangle \leftrightarrow |ex'\rangle$ transition [42]. Having $\Omega \gg g\sqrt{N}$, where g is the single-photon Rabi frequency of the cavity-coupled $|1\rangle \leftrightarrow |ex\rangle$ transition ensures that there is effectively no coupling of the atoms to the cavity field. In this way, atom-photon entanglement can be attempted with each atom sequentially as described previously.

The photons collected from the cavity are transmitted to either one of the ground stations or another satellite, depending on the specific location of the satellite in the repeater chain. In both cases, a linear optics BSM is performed at the destination to herald atom-atom entanglement, as shown in Fig. 1(b). The latter is carried out with a 50/50 beam splitter and single-photon detectors following the scheme of Ref. [38]. If the BSM is successful, meaning we have measured an early and a late photon, we have accomplished entanglement in an elementary link, that is, satellite-satellite or satellite-ground entanglement,

$$|\psi\rangle_{sp} \otimes |\psi\rangle_{sp} \xrightarrow{BSM} |\psi\rangle = \frac{1}{\sqrt{2}}(|01\rangle \pm |10\rangle). \tag{3}$$

The phase of the superposition is determined by which detectors record the photons. Since this information is known, it is possible to change the phase with local qubit operations, if necessary.

C. Entanglement swapping

Following the successful atom-atom entanglement generation of neighboring links in the setup, we carry out an entanglement swapping between the entangled atoms of the different links. Previous satellite-based quantum repeater schemes have considered photonic Bell measurements similar to the entanglement generation step [16,17,20] to achieve this. However, the downside of performing a photonic BSM is that it has an intrinsic failure probability of 50%, which has a detrimental effect on the overall rate of the repeater. To circumvent this, we consider nearly-deterministic Bell measurement between a pair of atoms through the Rydberg interaction. To do so, the atoms are spatially rearranged. This can be performed on a timescale of milliseconds [30,35], which is on the order of the communication time between segments for the parameters considered later. This is different from the situation in the entanglement generation step where the typical time scale of the local operations is on the microsecond scale for typical experimental parameters [35,36] and thus negligible compared with the communication time.

A Rydberg-mediated Controlled Z (CZ) gate between the two atoms [32,43,44] is assumed for the Bell measurement. Since the originally proposed schemes in Ref. [43], there have been a number of further developments to increase the performance of Rydberg-mediated two-atom gates [32,44], leading to experimentally reported gate fidelities exceeding 99% [34]. To illustrate the basic idea of how the Rydberg-interaction allows for a two-atom controlled phase gate, we focus, however, on one of the original schemes of Ref. [43], illustrated in Fig. 2(b) for simplicity. First, a π pulse is applied to the control atom, which makes the transition $|1\rangle \rightarrow |r\rangle$, where $|r\rangle$ is a Rydberg state with a high principal quantum number ($n \approx 60$). Then, a 2π pulse is applied to the target atom. If the control atom is in state $|0\rangle$, this pulse will make the transition $|1\rangle \rightarrow |r\rangle \rightarrow -|1\rangle$ on the target atom. However, if the control atom is in the Rydberg state, the Rydberg interaction will shift the transition out of resonance such that the target atoms remain essentially unperturbed by the pulse. A final π pulse brings the population of the control atom back to $|1\rangle$ and concludes the gate. This operation amounts ideally to a controlled phase gate between the atoms, which is sufficient to perform a BSM.

To realize a Bell measurement, it is necessary to apply a Hadamard gate on the target atom before the CZ gate and a Hadamard gate on the control atom after the gate, which can be done with two-photon Raman driving [30,41]. The qubit states are then measured by first driving the closed $|1\rangle \leftrightarrow |ex\rangle$ transition and collecting the emitted light, which detects if the atom is in the $|1\rangle$ state. If no light is detected, the atom is either in the $|0\rangle$ state, or it could have been lost from the trap. The latter can result from the rearrangement step, the two-atom gate, or simply from imperfect vacuum. To herald whether the atom was lost, a Raman drive is applied to bring the population from $|0\rangle$ to $|1\rangle$ followed by a second detection. If light is collected, the atom was in the $|0\rangle$ state, while if no light was collected, the atom is assumed lost. We note that this means that the Bell measurement is in fact not deterministic since there is a nonzero probability that the atom was lost, in which case the operation fails.

D. Performance

To evaluate the performance of the repeater protocol, we model a number of imperfections at both the quantum hardware level and in the optical transmission budget. In what follows, we describe these imperfections at a high level and refer to Appendix B and the Supplemental Material [45] for additional details of the modeling. At the quantum hardware level, we consider different imperfections in the entanglement generation, the quantum memories, and the entanglement swapping.

Entanglement generation: In the generation of spin-photon entanglement, we consider undesired two-photon emissions and imperfect coupling to the cavity mode. After the entangled photon is sent from the emitter to the receiver, a probabilistic optical BSM is performed. The photons interfering may not be perfectly indistinguishable, which is accounted for by including a nonunity visibility. The efficiency of the detector and the coupling losses from free space to fiber are also included in the link budget (see later). Moreover, dark counts can generate a "click" in the detectors, despite no photon being transmitted, which we include with a nonzero dark count probability.

Quantum memories: The atom-atom entanglement will decohere over time due to the dephasing of the spin state of the atoms. We model this as single-qubit dephasing channels acting on each atomic qubit, leading to an exponential decrease of coherence with time. Furthermore, the atoms can get lost from the traps due to imperfect vacuum, which we model as an erasure channel with an exponential decay of the qubit population with time.

Entanglement swapping: After entanglement between neighboring links is successfully achieved, we carry out the atomic Bell measurements in all the satellites of the chain to enable entanglement swapping to the ground stations. To account for imperfections in the CZ-gate, we assume that the gate succeeds perfectly with some probability p_{swap}, while with probability $1 - p_{\text{swap}}$ the swapping results in a "garbage" state with zero fidelity with the desired Bell state. In addition, we also include a finite probability that the atoms participating in the Bell measurement are lost, which also destroys the entanglement but is a heralded error.

Optical link budget: We compute free space propagation losses assuming a fundamental Gaussian beam under transmitter pointing jitter. The latter is assumed to be described by a radially varying Rayleigh probability distribution function. Furthermore, for satellite-to-ground links, we account for atmospheric effects such as Rayleigh scattering and turbulence-induced beam widening, operating in the weak turbulence regime due to the assumption of high-altitude ground stations. Finally, internal losses in the terminals, due to nonideal operation of the optical elements (i.e., absorption in lenses and mirrors) are included.

In our simulations, we consider two different satellites. One has the characteristics of the Micius satellite [24], namely, a telescope with a 15-cm radius and 0.41 μrad pointing error. In addition, we consider an improved second satellite, with a 50-cm-radius telescope. In both cases, the satellite orbit is at a height of 500 km from the surface of the Earth, the same as the Micius satellite, and both ground

stations have a 60-cm-radius telescope. We also assume the satellites to be in a "string of pearls" configuration following an equatorial orbit. The ground stations are assumed to be at a height of 2000 meters to avoid Mie scattering. Mie scattering is produced by particles of size comparable to the wavelength of light, mainly due to atmospheric aerosols. These particles are more abundant in the lower atmosphere and can be neglected for higher elevations [46].

As detailed in the Supplemental Material [45], we can derive an analytical estimate of the fidelity of final Bell pairs distributed between the ground stations taking into account all of the aforementioned errors and losses. To do this, we adopt a model where errors either lead to a completely dephased Bell state of the from $\rho_{\text{deph}} = (|01\rangle\langle 01| + |10\rangle\langle 10|)/2$ or end up in a nonspecified "garbage" density matrix ρ_{garb} with zero overlap with the desired target state $|\psi\rangle = (|01\rangle + |10\rangle)/\sqrt{2}$.

In our entanglement generation process, errors caused by two-photon events, memory dephasing, and imperfect optical visibility result in dephased Bell states. Since we operate in a regime with low transmission and dark count probabilities ($p_{\text{dark}}, p_T \ll 1$), we ignore terms proportional to $p_T p_{\text{dark}}$, neglecting any interference between dark counts and the signal. Dark counts thus only result in false heralding "clicks" where no signal photon was received, leading to the preparation of a nonentangled state of the corresponding memory qubits. To provide a lower bound on the entanglement quality, we model this nonentangled state as a garbage state with zero overlap with the desired Bell state. This allows us to express the density matrix describing the entangled pairs in the elementary links as $\rho_{\text{link}} = \alpha|\psi\rangle\langle\psi| + \beta\rho_{\text{deph}} + \gamma\rho_{\text{garb}}$. The dependence of the coefficients α, β, and γ on the physical parameters such as two-photon emission probability, transmission loss, dark counts, and memory coherence time are given in the Supplemental Material [45].

Finally, we model the imperfect entanglement swapping at the repeater nodes as succeeding with probability p_{swap} resulting in an error-free swap while with probability $1 - p_{\text{swap}}$, the entanglement swapping results in a garbage state. This allows us to obtain a compact expression of the final entangled state between the end nodes of the repeater

$$\rho_{\text{AB}} = p_{\text{swap}}^{n_{\text{sat}}}(A[n_{\text{sat}}]|\psi\rangle\langle\psi| + B[n_{\text{sat}}]\rho_{\text{deph}}) + C[n_{\text{sat}}]\rho_{\text{garb}} + \left(1 - p_{\text{swap}}^{n_{\text{sat}}}\right)(A[n_{\text{sat}}] + B[n_{\text{sat}}])\rho_{\text{garb}}, \tag{4}$$

where $p_{\text{swap}}^{n_{\text{sat}}}$ is the probability of no faulty entanglement swapping operations across the chain of n_{sat} satellites. The coefficients $A[n_{\text{sat}}]$, $B[n_{\text{sat}}]$, and $C[n_{\text{sat}}]$ can straightforwardly be found from combining $(n_{\text{sat}} + 1)$ states of the form ρ_{link} (see Appendix A for details). Note that, in general, the coefficients α, β, and γ will be different for each of the elementary links. From Eq. (A10), it follows that the fidelity of the final state with the target Bell state is $F_{\text{AB}} = p_{\text{swap}}^{n_{\text{sat}}} \frac{A[n_{\text{sat}}]+B[n_{\text{sat}}]/2}{A[n_{\text{sat}}]+B[n_{\text{sat}}]+C[n_{\text{sat}}]}$.

For the computation of the rate, we assume that N_{mem} photons are transmitted sequentially in each elementary link entangling attempt using $2N_{\text{mem}}$ atoms per emitter satellite, since each satellite covers two elementary links. In each attempt, we assume that the N_{mem} photons are emitted within a time assumed to be negligible compared with the communication time between the links, which is on the order of milliseconds. We therefore set the repetition time of the entangling attempt to match the longest communication time between links in the repeater chain.

After each attempt, the entanglement in a link is either swapped if the neighboring link is also successful or discarded before a new attempt is made. We choose this mode of operation because for quantum memories with second-long coherence times, as considered in this work, the communication time between elementary links is too long to maintain high-fidelity entanglement by storing successful links for multiple entanglement attempts. It is therefore desirable to have enough multiplexing to ensure near-deterministic entanglement generation in the elementary links [47].

To estimate the rate of the repeater, we first consider the probability of generating n Bell pairs in a single elementary link, which is simply

$$p_{(g,s)}(n) = \binom{N_{\text{mem}}}{n} p_{\text{link},(g,s)}^{n}(1 - p_{\text{link},(g,s)})^{N_{\text{mem}}-n}, \tag{5}$$

where $p_{\text{link},(g,s)}$ is the success probability per photon for ground-satellite (g) or satellite-satellite links (s). This expression is valid in the regime where the optical transmission is limited by beam divergence rather than pointing errors, since the latter can induce correlated errors, whereas the binomial distribution assumes uncorrelated loss. We verify that this is the case for realistic pointing errors through Monte Carlo simulations of the distribution of entangled pairs in an elementary link (see Supplemental Materials for details [45]). Since the number of entangled pairs between the ground stations will be limited by the link with the smallest number of successful pairs, we can express the probability of generating n entangled pairs between the ground stations, assuming deterministic swapping, as

$$p(n) = \left(\sum_{i=0}^{n_{\text{sat}}-1} \binom{n_{\text{sat}}-1}{i} p_s(n)^i p_s(>n)^{n_{\text{sat}}-(i+1)}\right) \cdot \left(\sum_{j=0}^{2} \binom{2}{j} p_g(n)^j p_g(>n)^{2-j}\right) - p_s(>n)^{n_{\text{sat}}-1} p_g(>n)^2, \tag{6}$$

where $p_{(g,s)}(>n) = \sum_{i=n+1}^{N_{\text{mem}}} p_{(g,s)}(i)$.

Since the entanglement swapping is only near-deterministic due to the possibility of atom loss, we need to include the probability of losing some of these pairs due to failed entanglement swappings. This modifies the probability for establishing n entangled pairs between the ground stations to

$$p_f(n) = \sum_{i=n}^{N_{\text{mem}}} \binom{i}{n} p(i)(1 - p_{\text{loss}})^n p_{\text{loss}}^{i-n}, \tag{7}$$

where p_{loss} is the probability of unsuccessfully combining the entangled pairs in the elementary links to achieve an entangled pair between the ground stations due to loss of at least one atom in any of the elementary link pairs. The final average rate of the repeater is then estimated as

$$R = \frac{\sum_{i=1}^{N_{\text{mem}}} i p_f(i)}{T_{\text{com}}}, \tag{8}$$

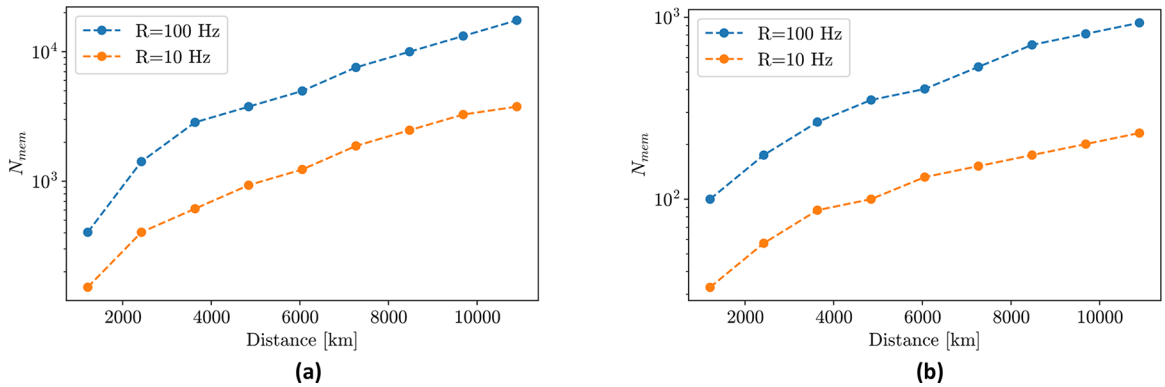

FIG. 3. Multiplexing capabilities required to reach a rate of 10 Hz (orange) or 100 Hz (blue) and a fidelity of 0.9 in the entanglement distribution protocol in a satellite chain of five satellites. (a) Number of memory modes, N_{mem}, needed in a satellite with the characteristics of Micius, that is, the same size of the telescope ($r = 0.15$ m), pointing error ($\sigma = 0.41$ μrad), and height ($h = 500$ km), as a function of the distance between ground stations. (b) Number of memory modes, N_{mem}, in the text, needed in a satellite with a bigger telescope radius than Micius ($r = 0.5$ m) as a function of the distance between ground stations.

where we have assumed that the repetition rate is set by T_{com}, which is the longest round-trip communication time between elementary links. Additional details about the calculation of the rate and fidelity can be found in the Supplemental Material, where we provide detailed expressions for $p_{\text{link},(g,s)}$, p_{loss}, and T_{com}.

Rather than using the rate analysis described previously to estimate the achievable rate and fidelity for a fixed number of atoms, N_{mem}, we instead estimate the number of atoms needed to achieve a certain target rate and fidelity. We do this to get a sense of the multiplexing capabilities needed to reach fidelities above 90% compatible with secret key distillation [48,49], and rates above 10 Hz (100 Hz) such that at least 10 (100) entangled pairs could be distributed within the second-long memory time that we assume for the ground-state memories. Fidelities above 50% indicate the presence of entanglement. Since the satellites are moving in orbit, the rate is estimated as the average rate during the time window where ground-satellite communication is possible. This communication window is about 5 minutes per satellite pass above the ground stations for the satellite height of 500 km considered here.

In Fig. 3, we plot the necessary number of memory modes per repeater node, to reach a certain rate of entanglement between the ground stations, in this case 10 Hz or 100 Hz, and a fidelity $\geqslant 0.9$ of the final Bell pair as a function of distance, assuming a chain of five satellites. The parameters considered in the simulation are shown in Table I.

TABLE I. Assumed values of the parameters in the model. The assumed values are compatible with current or near-term technology. The parameters that differ from those shown in this table are indicated in the figures. The collection efficiency is defined as $\eta_{\text{coll}} = p\eta_{\text{cav,coll}}$, where $p = 0.99$ is the probability of emitting in the cavity mode, and $\eta_{\text{cav,coll}} = 0.5$ is the collection efficiency from the cavity to free space. The effective loss coherence times depend on the quality of the vacuum in the atomic memories and are assumed to be higher for ground stations than on the satellites. The values of the transmission probability between satellites shown are the ones for the shortest distance between ground stations (∼1300 km) and for the longest one(∼12 000 km) to provide a sense of the relevant regime.

Parameters considered for the simulations		
Prob. of the emitter to emit a single photon	p_1	0.99
Prob. of the emitter to emit two photons	p_2	0.002
Collection efficiency	η_{coll}	0.49
Visibility of the photons	$\mathcal{V}$	0.999
Prob. of losing an atom in the entanglement swap	$p_{\text{loss,swap}}$	0.1
Effective loss time in satellite	$T_{\text{loss,sat}}$	0.01 s
Effective loss time in ground station	$T_{\text{loss,gstat}}$	1.5 s
Fidelity of the entanglement swap	p_{swap}	0.995
Dark detection probability	p_{dark}	10^{-6}
Decoherence time in satellite	$\tau_{\text{c,sat}}$	1.5 s
Decoherence time in ground station	$\tau_{\text{c,gstat}}$	10 s
Photon detection efficiency	η	0.98
Transmission probabilities in the elementary links		
Trans. prob. sat.-ground. ($r = 0.15$ m)	$p_{\text{T,sat-ground}}$	0.14
Trans. prob. sat.-ground. ($r = 0.5$ m)	$p_{\text{T,sat-ground}}$	0.33
Trans. prob. sat.-sat. ($r = 0.15$ m)	$p_{\text{T,sat-sat}}$	0.052–0.0007
Trans. prob. sat.-sat. ($r = 0.5$ m)	$p_{\text{T,sat-sat}}$	0.55–0.03

From the comparison of Figs. 3(a) and 3(b), it is seen that increasing the radius of the satellite mirrors relaxes the multiplexing requirements up to two orders of magnitude. While the Micius-like satellite requires more than 1000 memory modes to achieve a rate of 100 Hz for a distance of 3500 km between ground stations, the upgraded satellite only requires ∼200 memories. Additionally, the upgraded satellite only requires around 1000 memory modes to reach a rate of 100 Hz over distances $\geqslant$ 8000 km. This is an order of magnitude less than found in optical BSM architectures for similar satellite characteristics [16].

We chose to target a final fidelity of $\geqslant 0.9$ since this allows for direct extraction of secure encryption keys through QKD [48,49]. If higher fidelity entanglement is required, this can, in principle be achieved through entanglement purification [50]. Increasing the rate from the targeted 10 Hz or 100 Hz can be achieved by increasing the amount of multiplexing. Increasing the number of memory modes in Fig. 3 by a certain factor will result in roughly the same increase in rate.

Table I shows the assumed quality of the hardware and quantum operations, for example, the entanglement swapping quality and photon detection efficiency, to reach a final fidelity $\geqslant 0.9$. Lower error budgets in the quantum hardware will naturally increase the performance of the repeater. While errors at the 0.1% level are within reach of current neutral atom-based hardware, entanglement purification techniques could also be employed to leverage the effect of nonperfect operations at the expense of a slower distribution rate.

III. CONCLUSION

In summary, we have proposed a satellite-assisted quantum repeater architecture based on individually trapped alkali atoms, which has several desirable features for functioning as quantum payloads. In particular, the ability to perform nearly deterministic BSMs with Rydberg-mediated two-qubit gates significantly lowers the amount of multiplexing needed to establish entanglement at continental distances compared with protocols based on probabilistic linear optics BSMs [16]. Additionally, the use of atoms as single-photon sources circumvents the need for entangled photon sources and absorptive quantum memories.

We developed a simple but accurate analytical model where we included the main imperfections of the quantum hardware and the optical link, assuming high-altitude ground stations, and consequently working in a regime of weak atmospheric turbulence. This model allowed us to compute how expensive, in the sense of the number of memory modes per repeater station, it is to get high-fidelity entanglement at continental distances using the setup we propose. From this model, we estimated that a chain of five satellites with a 50-cm radius telescope, enables high-fidelity ($F \geqslant 0.9$) entanglement at a rate of 100 Hz with less than 200 atoms per repeater station at a range of 1500 km.

We believe that our model can be readily adapted to provide first-order estimates of the performance for other satellite-assisted quantum repeater architectures based on heralded entanglement generation and entanglement swapping, also with different quantum hardware. This is due to the characterization of the effect of the physical errors into simple lower-bound estimates of the fidelity of the final state. Notably, our model allows for easy and fast simulation of long quantum repeater chains in contrast to Monte Carlo-based simulations [18], where the computational overhead increases rapidly with the length of the repeater chain.

In addition to the promise of long-distance entanglement distribution, satellite-assisted quantum repeaters also open up new tools for more fundamental tests of nature. In particular, the atomic hardware considered here presents new opportunities for quantum-enhanced sensor networks relevant for searches for topological dark matter [51], global time-keeping [4], and tests of the interplay between gravity and quantum mechanics [52].

ACKNOWLEDGMENTS

We acknowledge helpful discussions with Rudolf Saathof, Bob Dirks, and Gustavo Castro do Amaral. We acknowledge funding from the Quantum Software Consortium (NWO Zwaartekracht Grant No. 024.003.037). J.B. acknowledges support from The AWS Quantum Discovery Fund at the Harvard Quantum Initiative. A.S. acknowledges the support of Danmarks Grundforskningsfond (DNRF 139, Hy-Q Center for Hybrid Quantum Networks).

DATA AVAILABILITY

The code and data for the results of this paper are openly available on 4TU.ResearchData: "Data underlying the publication "Satellite-assisted quantum communication with single photon sources and atomic memories," at Ref. [53].

APPENDIX A: ENTANGLEMENT SWAPPING

In this Appendix, we give a more detailed calculation of how we carry out the entanglement swapping. Before the entanglement swap, the state of each elementary link is of the form:

$$\alpha|\psi\rangle\langle\psi| + \beta\rho_{\text{deph}} + \gamma\rho_{\text{garb}}, \tag{A1}$$

where α, β, and γ are the probabilities of getting the desired entangled state, a dephased state, and a garbage state, respectively, after taking into account imperfection in the source, the transmission loss through free space and the atmosphere, the photonic Bell measurements, and the decoherence of the quantum memories. The full expression of these parameters can be found in the Supplemental Material [45].

The input of the first entanglement swapping is the following:

$$\begin{aligned}&(\alpha_0|\psi\rangle\langle\psi| + \beta_0\rho_{\text{deph}} + \gamma_0\rho_{\text{garb}})_{12}\\ &\otimes(\alpha_1|\psi\rangle\langle\psi| + \beta_1\rho_{\text{deph}} + \gamma_1\rho_{\text{garb}})_{34},\end{aligned} \tag{A2}$$

which is followed by a CNOT gate on qubits 2 –3, a Hadamard gate on qubit 2, and the measurement of both qubits. In this expression, we have included a subindex on the coefficients $\{\alpha, \beta, \gamma\}$, since the states of the elementary links can, in general, be different due to, for example, different transmission probabilities.

After a successful (i.e., no atom loss detected) entanglement swapping operation, the swapped state will be of the form

$$A[1]|\psi\rangle\langle\psi| + B[1]\rho_{\text{deph}} + C[1]\rho_{\text{garb}}, \tag{A3}$$

where

$$A[1] = \alpha_0\alpha_1, \tag{A4}$$

$$B[1] = \beta_0(\alpha_1 + \beta_1) + \alpha_0\beta_1, \tag{A5}$$

$$C[1] = \gamma_0(\alpha_1 + \beta_1) + \gamma_1(\alpha_0 + \beta_0) + p_2\gamma_0\gamma_1. \tag{A6}$$

The state after performing n entanglement swaps is described by the recursive expressions:

$$A[n] = A[n-1]\alpha_n, \tag{A7}$$

$$B[n] = A[n-1]\beta_n + B[n-1](\alpha_n + \beta_n), \tag{A8}$$

$$\begin{aligned} C[n] = {} & \gamma_n(A[n-1] + B[n-1]) \\ & + C[n-1](\alpha_n + \beta_n + p_2\gamma_n). \end{aligned} \tag{A9}$$

Lastly, we also consider the fidelity of the entanglement swapping operation. We assume that with probability, p_{swap}, the entanglement swapping operation is perfect, while with probability $1 - p_{\text{swap}}$, the resulting state is a garbage state, which amounts to a lower bound on the fidelity of the swapped state. Thus, after n_{sat} entanglement swaps (the number of entanglement swaps is equal to the number of satellites), the end-to-end entangled pair will be of the form:

$$\begin{aligned} \rho_{\text{AB}} = {} & p_{\text{swap}}^{n_{\text{sat}}}(A[n_{\text{sat}}]|\psi\rangle\langle\psi| + B[n_{\text{sat}}]\rho_{\text{deph}}) \\ & + \left(\left(1 - p_{\text{swap}}^{n_{\text{sat}}}\right)(A[n_{\text{sat}}] + B[n_{\text{sat}}]) + C[n_{\text{sat}}]\right)\rho_{\text{garb}}. \end{aligned} \tag{A10}$$

APPENDIX B: MODELING OF ERRORS

In this Appendix, we provide more details on our model of hardware imperfections and transmission loss in the satellite repeater chain. Specifically, we describe how we model two-photon emission errors, dark counts, quantum memory dephasing, and atom loss. Finally, we describe our model of the optical transmission, including beam divergence, pointing jitter, and atmospheric absorption. Additional details can be found in the Supplemental Material [45].

In the first step of the protocol for establishing entanglement between the spin of the emitter and the photon, we take into account two-photon emissions and that the photons may not be emitted into the cavity mode. The collected photons are sent to the closest satellite or to the ground station for the spin-spin entanglement generation. The photons will reach their destination with probability p_{T}, computed using the optical link budget explained later in this section. These free-space and atmospheric losses are modeled as a fictitious beam splitter with transmission p_{T}. The transmission of a single-photon is modeled as follows:

$$\hat{a}^\dagger_{\text{ph}}|0\rangle_{\text{ph}}|0\rangle_{\text{E}} \to \sqrt{p_{\text{T}}}\hat{a}^\dagger_{\text{ph}}|0\rangle_{\text{ph}}|0\rangle_{\text{E}} + \sqrt{1 - p_{\text{T}}}\hat{a}^\dagger_{\text{E}}|0\rangle_{ph}|0\rangle_{\text{E}}, \tag{B1}$$

where $\hat{a}^\dagger_{\text{ph}}$ is the creation operator for the collected mode, while $\hat{a}^\dagger_{\text{E}}$ is the creation of a noncollected (environment) photon. Once the photon reaches the receiver, a photonic BSM is performed between the emitted photon and a photon emitted from an atom in the receiver system. The two photons may not be perfectly indistinguishable and the efficiency of the single-photon detectors and the coupling from free space to fiber is not perfect. These factors are added to the model as the visibility of the photons, the detector, and the coupling efficiency. The photon detection efficiency of the spaceborne superconducting nanowire single photon detectors (SNSPD) is considered to be the same as the ones previously reported in ground-based SNSPDs [54,55]. The authors expect that such performances are possible in the near future, by leveraging the longstanding heritage of other cryogenic detectors in space [56]. Moreover, dark counts can generate a "click" in the detectors, when there is no photon to measure, which is considered in the dark count probability. The photonic BSM is modeled as a 50/50 beam splitter where just single-photon emissions are considered indistinguishable, leading to interference terms. In other words, we do not consider interference between photons from two-photon emissions since these will likely be emitted with very different temporal envelopes, resulting in negligible interference effects. As a result of these imperfections, the final atom-atom entangled states are captured by probabilistic mixtures of the ideal Bell state, a dephased state, and a nonspecified garbage state with fidelity zero (which includes, e.g., the $|00\rangle$ and $|11\rangle$ states) as specified in the supplemental material [45].

The entanglement is "stored" in the hyperfine spin of the Rubidium atoms but decoheres with time. We model this as a dephasing channel, where the coherence (off-diagonal terms of the density matrix) decays exponentially with time as $\exp(-t/\tau_c)$, where τ_c is the coherence time of the atoms (assumed different for ground and satellites as detailed in Table I). In addition, we assume that the atoms can get lost due to imperfect vacuum. We model this by assuming that with probability $\exp(-t/T_{\text{loss}})$ an atom is lost after a time t, where T_{loss} is an effective loss time (also assumed different for satellite and ground).

After entanglement between elementary links is successfully achieved, we carry out the entanglement swapping in all the satellites of the chain. To do so, the tweezers move the atoms that have established entanglement with their counterparts at the end of their respective elementary links to the top positions of the cavity, such that we know where the successfully entangled atoms are. The imperfections of the entanglement swapping are modeled as described in the main text.

As shown in Fig. 4(b), we include a number of imperfections and loss for the optical link budget. The free-space propagation losses are computed considering a fundamental Gaussian beam under transmitter pointing jitter. The latter is assumed to be described by a radially varying Rayleigh probability distribution function, which is the result of the combination of centered Gaussian probability density functions in both the vertical and horizontal directions. The joint Gaussian probability density function of the pointing jitter is

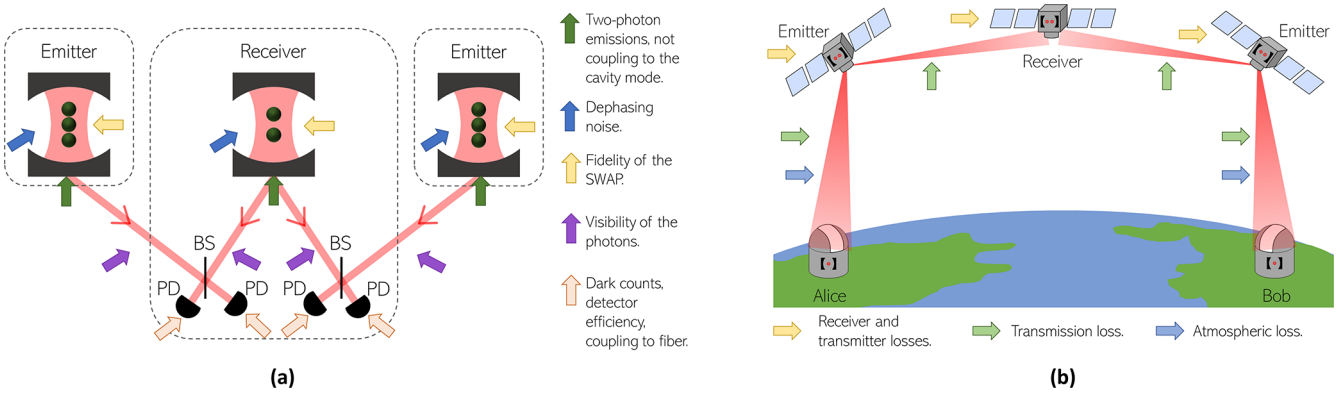

FIG. 4. Errors considered in the protocol. (a) Schematic representation of the quantum setup used and possible errors that can happen. Two-photon emissions and imperfect coupling to the cavity mode are taken into account when modeling the atom-photon entanglement generation. Dark counts, detector efficiency, and coupling to the fiber are included as imperfections in the Bell state measurements carried out in the receivers. Nonperfect visibility of the photons involved in the Bell state measurement is also included. Finally, we include the dephasing of the atoms and imperfections of the entanglement swapping operation. (b) Schematic representation of the transmission losses. In the satellite-satellite link, we take into account transmission losses due to the propagation of the Gaussian beam and the pointing jitter of the emitter. In the satellite-ground station link, we also consider the effect of the atmosphere, that is, the Rayleigh scattering due to molecules. Additionally, losses originated in the terminals are also added to the model.

given by

$$f(x_0, y_0; \sigma) = \frac{1}{2\pi\sigma^2} \exp\left(-\frac{x_0^2 + y_0^2}{2\sigma^2}\right), \tag{B2}$$

where x_0 and y_0 are the coordinates of the pointing error in the receiver's aperture plane, and σ is the pointing jitter's standard deviation for both directions. The effect of pointing errors is that the center of the Gaussian beam profile is not aligned with the center of the receiver. In the regime where the width σ of the pointing jitter is small compared with the beam waist at the receiver, w, the effect of pointing jitter will be small and the transmission will be dominated by beam divergence. This allows us to use the binomial distribution approximation of the number of successful pairs in an elementary link used in our model [see Eq. (5)] using the average transmission probability with respect to the pointing jitter. From numerical Monte Carlo simulations, we find that, for $w/\sigma \geqslant 10$, the binomial distribution approximation is good (see the Supplemental Material for further details [45]). For realistic pointing errors and beam focusing characteristics [57], this requirement is fulfilled [45]. In satellite-to-ground links, the atmospheric effects have been included in the model using simulated atmospheric transmission from Ref. [58]. We consider that the ground stations are at an altitude higher than 2000 meters [59], that the telescope on the ground has a diameter of 2 meters, allowing for aperture averaging effects of atmospheric turbulence scintillation [37,60], and that weak turbulence conditions are satisfied [37]. Given these three factors, the effects of atmospheric turbulence-induced scintillation will be negligible, and the beam wandering will be dominated by transmitter pointing jitter.

[1] C. H. Bennett and G. Brassard, Quantum cryptography: Public key distribution and coin tossing, Theor. Comput. Sci. **560**, 7 (2014).
[2] A. K. Ekert, Quantum cryptography based on Bell's theorem, Phys. Rev. Lett. **67**, 661 (1991).
[3] S. Pirandola, U. L. Andersen, L. Banchi, M. Berta, D. Bunandar, R. Colbeck, D. Englund, T. Gehring, C. Lupo, C. Ottaviani, J. L. Pereira, M. Razavi, J. S. Shaari, M. Tomamichel, V. C. Usenko, G. Vallone, P. Villoresi, and P. Wallden, Advances in quantum cryptography, Adv. Opt. Photon. **12**, 1012 (2020).
[4] P. Kómár, E. M. Kessler, M. Bishof, L. Jiang, A. S. Sørensen, J. Ye, and M. D. Lukin, A quantum network of clocks, Nat. Phys. **10**, 582 (2014).
[5] X. Guo, C. R. Breum, J. Borregaard, S. Izumi, M. V. Larsen, T. Gehring, M. Christandl, J. S. Neergaard-Nielsen, and U. L. Andersen, Distributed quantum sensing in a continuous-variable entangled network, Nat. Phys. **16**, 281 (2020).
[6] L.-Z. Liu, Y.-Z. Zhang, Z.-D. Li, R. Zhang, X.-F. Yin, Y.-Y. Fei, L. Li, N.-L. Liu, F. Xu, Y.-A. Chen, and J.-W. Pan, Distributed quantum phase estimation with entangled photons, Nat. Photon. **15**, 137 (2021).
[7] H. Buhrman and H. Röhrig, Distributed quantum computing, in *Mathematical Foundations of Computer Science 2003*, Lecture Notes in Computer Science, edited by B. Rovan and P. Vojtáš (Springer, Bratislava, Slovakia, 2003), pp. 1–20.
[8] Z. Tang, P. Zhang, W. O. Krawec, and L. Wang, Quantum networks for resilient power grids: Theory and simulated evaluation, IEEE Trans. Power Syst. **38**, 1189 (2023).
[9] B. C. Nichol, R. Srinivas, D. P. Nadlinger, P. Drmota, D. Main, G. Araneda, C. J. Ballance, and D. M. Lucas, An elementary quantum network of entangled optical atomic clocks, Nature (London) **609**, 689 (2022).
[10] W. K. Wootters and W. H. Zurek, A single quantum cannot be cloned, Nature (London) **299**, 802 (1982).

[11] L. M. Duan, M. D. Lukin, J. I. Cirac, and P. Zoller, Long-distance quantum communication with atomic ensembles and linear optics, Nature (London) **414**, 413 (2001).

[12] N. Sangouard, C. Simon, H. de Riedmatten, and N. Gisin, Quantum repeaters based on atomic ensembles and linear optics, Rev. Mod. Phys. **83**, 33 (2011).

[13] S. Muralidharan, J. Kim, N. Lütkenhaus, M. D. Lukin, and L. Jiang, Ultrafast and fault-tolerant quantum communication across long distances, Phys. Rev. Lett. **112**, 250501 (2014).

[14] W. J. Munro, A. M. Stephens, S. J. Devitt, K. A. Harrison, and K. Nemoto, Quantum communication without the necessity of quantum memories, Nat. Photon. **6**, 777 (2012).

[15] L. de Forges de Parny, O. Alibart, J. Debaud, S. Gressani, A. Lagarrigue, A. Martin, A. Metrat, M. Schiavon, T. Troisi, E. Diamanti, P. Gélard, E. Kerstel, S. Tanzilli, and M. Van Den Bossche, Satellite-based quantum information networks: Use cases, architecture, and roadmap, Commun. Phys. **6**, 12 (2023).

[16] C. Liorni, H. Kampermann, and D. Bruß, Quantum repeaters in space, New J. Phys. **23**, 053021 (2021).

[17] M. Gündoğan, J. S. Sidhu, V. Henderson, L. Mazzarella, J. Wolters, D. K. L. Oi, and M. Krutzik, Proposal for space-borne quantum memories for global quantum networking, npj Quantum Inf. **7**, 128 (2021).

[18] J. Wallnöfer, F. Hahn, M. Gündoğan, J. S. Sidhu, F. Wiesner, N. Walk, J. Eisert, and J. Wolters, Simulating quantum repeater strategies for multiple satellites, Commun. Phys. **5**, 169 (2022).

[19] S. Khatri, A. J. Brady, R. A. Desporte, M. P. Bart, and J. P. Dowling, Spooky action at a global distance: Analysis of space-based entanglement distribution for the quantum internet, npj Quantum Inf. **7**, 4 (2021).

[20] K. Boone, J.-P. Bourgoin, E. Meyer-Scott, K. Heshami, T. Jennewein, and C. Simon, Entanglement over global distances via quantum repeaters with satellite links, Phys. Rev. A **91**, 052325 (2015).

[21] D. L. Bakker, Y. Jong, B. P. F. Dirks, and G. C. Amaral, A best-path approach to the design of a hybrid space–ground quantum network with dynamic constraints, Photonics **11**, 268 (2024).

[22] J. Yin, Y. Cao, Y.-H. Li, J.-G. Ren, S.-K. Liao, L. Zhang, W.-Q. Cai, W.-Y. Liu, B. Li, H. Dai, M. Li, Y.-M. Huang, L. Deng, L. Li, Q. Zhang, N.-L. Liu, Y.-A. Chen, C.-Y. Lu, R. Shu, C.-Z. Peng *et al.*, Satellite-to-ground entanglement-based quantum key distribution, Phys. Rev. Lett. **119**, 200501 (2017).

[23] S.-K. Liao, W.-Q. Cai, J. Handsteiner, B. Liu, J. Yin, L. Zhang, D. Rauch, M. Fink, J.-G. Ren, W.-Y. Liu, Y. Li, Q. Shen, Y. Cao, F.-Z. Li, J.-F. Wang, Y.-M. Huang, L. Deng, T. Xi, L. Ma, T. Hu *et al.*, Satellite-relayed intercontinental quantum network, Phys. Rev. Lett. **120**, 030501 (2018).

[24] J. Yin, Y.-H. Li, S.-K. Liao, M. Yang, Y. Cao, L. Zhang, J.-G. Ren, W.-Q. Cai, W.-Y. Liu, S.-L. Li, R. Shu, Y.-M. Huang, L. Deng, L. Li, Q. Zhang, N.-L. Liu, Y.-A. Chen, C.-Y. Lu, X.-B. Wang, F. Xu *et al.*, Entanglement-based secure quantum cryptography over 1,120 kilometres, Nature (London) **582**, 501 (2020).

[25] A. Anwar, C. Perumangatt, A. Villar, A. Lohrmann, and A. Ling, Development of compact entangled photon-pair sources for satellites, Appl. Phys. Lett. **121**, 220503 (2022).

[26] C. Schimpf, M. Reindl, F. Basso Basset, K. D. Jöns, R. Trotta, and A. Rastelli, Quantum dots as potential sources of strongly entangled photons: Perspectives and challenges for applications in quantum networks, Appl. Phys. Lett. **118**, 100502 (2021).

[27] K. C. Chen, P. Dhara, M. Heuck, Y. Lee, W. Dai, S. Guha, and D. Englund, Zero-added-loss entangled-photon multiplexing for ground- and space-based quantum networks, Phys. Rev. Appl. **19**, 054029 (2023).

[28] Q. Zhang, X.-H. Bao, C.-Y. Lu, X.-Q. Zhou, T. Yang, T. Rudolph, and J.-W. Pan, Demonstration of a scheme for the generation of "event-ready" entangled photon pairs from a single-photon source, Phys. Rev. A **77**, 062316 (2008).

[29] J. McKeever, A. Boca, A. D. Boozer, R. Miller, J. R. Buck, A. Kuzmich, and H. J. Kimble, Deterministic generation of single photons from one atom trapped in a cavity, Science **303**, 1992 (2004).

[30] D. Bluvstein, H. Levine, G. Semeghini, T. T. Wang, S. Ebadi, M. Kalinowski, A. Keesling, N. Maskara, H. Pichler, M. Greiner, V. Vuletić, and M. D. Lukin, A quantum processor based on coherent transport of entangled atom arrays, Nature (London) **604**, 451 (2022).

[31] A. W. Young, W. J. Eckner, W. R. Milner, D. Kedar, M. A. Norcia, E. Oelker, N. Schine, J. Ye, and A. M. Kaufman, Half-minute-scale atomic coherence and high relative stability in a tweezer clock, Nature (London) **588**, 408 (2020).

[32] H. Levine, A. Keesling, G. Semeghini, A. Omran, T. T. Wang, S. Ebadi, H. Bernien, M. Greiner, V. Vuletić, H. Pichler, and M. D. Lukin, Parallel implementation of high-fidelity multiqubit gates with neutral atoms, Phys. Rev. Lett. **123**, 170503 (2019).

[33] Z. Fu, P. Xu, Y. Sun, Y.-Y. Liu, X.-D. He, X. Li, M. Liu, R.-B. Li, J. Wang, L. Liu, and M.-S. Zhan, High-fidelity entanglement of neutral atoms via a rydberg-mediated single-modulated-pulse controlled-phase gate, Phys. Rev. A **105**, 042430 (2022).

[34] S. J. Evered, D. Bluvstein, M. Kalinowski, S. Ebadi, T. Manovitz, H. Zhou, S. H. Li, A. A. Geim, T. T. Wang, N. Maskara, H. Levine, G. Semeghini, M. Greiner, V. Vuletić, and M. D. Lukin, High-fidelity parallel entangling gates on a neutral-atom quantum computer, Nature (London) **622**, 268 (2023).

[35] W. Huie, S. G. Menon, H. Bernien, and J. P. Covey, Multiplexed telecommunication-band quantum networking with atom arrays in optical cavities, Phys. Rev. Res. **3**, 043154 (2021).

[36] J. P. Covey, H. Weinfurter, and H. Bernien, Quantum networks with neutral atom processing nodes, npj Quantum Inf. **9**, 90 (2023).

[37] L. C. Andrews and R. L. Phillips, *Laser Beam Propagation Through Random Media* (SPIE, Bellingham, WA, 2005).

[38] S. D. Barrett and P. Kok, Efficient high-fidelity quantum computation using matter qubits and linear optics, Phys. Rev. A **71**, 060310 (2005).

[39] C. Cabrillo, J. I. Cirac, P. García-Fernández, and P. Zoller, Creation of entangled states of distant atoms by interference, Phys. Rev. A **59**, 1025 (1999).

[40] E. Deist, J. A. Gerber, Y.-H. Lu, J. Zeiher, and D. M. Stamper-Kurn, Superresolution microscopy of optical fields using tweezer-trapped single atoms, Phys. Rev. Lett. **128**, 083201 (2022).

[41] H. Levine, D. Bluvstein, A. Keesling, T. T. Wang, S. Ebadi, G. Semeghini, A. Omran, M. Greiner, V. Vuletić, and M. D. Lukin, Dispersive optical systems for scalable Raman driving of hyperfine qubits, Phys. Rev. A **105**, 032618 (2022).

[42] Y. Li and J. Thompson, High-rate and high-fidelity modular interconnects between neutral atom quantum processors, PRX Quantum **5**, 020363 (2024).

[43] D. Jaksch, J. I. Cirac, P. Zoller, S. L. Rolston, R. Côté, and M. D. Lukin, Fast quantum gates for neutral atoms, Phys. Rev. Lett. **85**, 2208 (2000).

[44] S. Jandura and G. Pupillo, Time-optimal two- and three-qubit gates for rydberg atoms, Quantum **6**, 712 (2022).

[45] See Supplemental Material at http://link.aps.org/supplemental/10.1103/z1vn-11m5 for the quantum and optical hardware's mathematical model referenced in the text, which include Ref. [53].

[46] E. Brattich, E. Serrano Castillo, F. Giulietti, J.-B. Renard, S. N. Tripathi, K. Ghosh, G. Berthet, D. Vignelles, and L. Tositti, Measurements of aerosols and charged particles on the BEXUS18 stratospheric balloon, Ann. Geophys. **37**, 389 (2019).

[47] O. A. Collins, S. D. Jenkins, A. Kuzmich, and T. A. B. Kennedy, Multiplexed memory-insensitive quantum repeaters, Phys. Rev. Lett. **98**, 060502 (2007).

[48] N. Gisin, G. Ribordy, W. Tittel, and H. Zbinden, Quantum cryptography, Rev. Mod. Phys. **74**, 145 (2002).

[49] F. Xu, X. Ma, Q. Zhang, H.-K. Lo, and J.-W. Pan, Secure quantum key distribution with realistic devices, Rev. Mod. Phys. **92**, 025002 (2020).

[50] M. Victora, S. Tserkis, S. Krastanov, A. S. de la Cerda, S. Willis, and P. Narang, Entanglement purification on quantum networks, Phys. Rev. Res. **5**, 033171 (2023).

[51] A. Belenchia, M. Carlesso, Ömer Bayraktar, D. Dequal, I. Derkach, G. Gasbarri, W. Herr, Y. L. Li, M. Rademacher, J. Sidhu, D. K. Oi, S. T. Seidel, R. Kaltenbaek, C. Marquardt, H. Ulbricht, V. C. Usenko, L. Wörner, A. Xuereb, M. Paternostro, and A. Bassi, Quantum physics in space, Phys. Rep. **951**, 1 (2022) .

[52] D. E. Bruschi, C. Sabén, A. White, V. Baccetti, D. K. L. Oi, and I. Fuentes, Testing the effects of gravity and motion on quantum entanglement in space-based experiments, New J. Phys. **16**, 053041 (2014).

[53] V. Dominguez Tubio, M. Badas Aldecocea, J. van Dam, A. Sorensen, and J. Borregaard, Data underlying the publication "satellite-assisted quantum communication with single photon sources and atomic memories" (2024), https://doi.org/10.4121/61635423-89d3-46cb-b9bc-bc06f158b9a5.

[54] D. V. Reddy, R. R. Nerem, S. W. Nam, R. P. Mirin, and V. B. Verma, Superconducting nanowire single-photon detectors with 98% system detection efficiency at 1550 nm, Optica **7**, 1649 (2020) .

[55] I. Esmaeil Zadeh, J. W. N. Los, R. B. M. Gourgues, V. Steinmetz, G. Bulgarini, S. M. Dobrovolskiy, V. Zwiller, and S. N. Dorenbos, Single-photon detectors combining high efficiency, high detection rates, and ultra-high timing resolution, APL Photonics **2**, 111301 (2017).

[56] Y. Han and A. Zhang, Cryogenic technology for infrared detection in space, Sci. Rep. **12**, 2349 (2022).

[57] A. Carrasco-Casado, K. Shiratama, D. Kolev, P. Trinh, T. Fuse, S. Fuse, K. Kawaguchi, Y. Hashimoto, M. Hyodo, T. Sakamoto, T. Kunisada, and M. Toyoshima, Prototype development and validation of a beam-divergence control system for free-space laser communications, Front. Phys. **10**, 878488 (2022).

[58] D. Giggenbach and A. Shrestha, Atmospheric absorption and scattering impact on optical satellite-ground links, Int. J. Satell. Commun. Netw. **40**, 157 (2022).

[59] J. Yin, Y. Cao, Y.-H. Li, S.-K. Liao, L. Zhang, J.-G. Ren, W.-Q. Cai, W.-Y. Liu, B. Li, H. Dai, G.-B. Li, Q.-M. Lu, Y.-H. Gong, Y. Xu, S.-L. Li, F.-Z. Li, Y.-Y. Yin, Z.-Q. Jiang, M. Li, J.-J. Jia *et al.*, Satellite-based entanglement distribution over 1200 kilometers, Science **356**, 1140 (2017).

[60] D. Vasylyev, W. Vogel, and F. Moll, Satellite-mediated quantum atmospheric links, Phys. Rev. A **99**, 053830 (2019).